Diffraction limited 195-W continuous wave laser emission at 2.09 μm from a Tm3+, Ho3+-codoped single-oscillator monolithic fiber laser

Arnaud Motard, Christophe Louot, Thierry Robin, Benoit Cadier, Inka Manek-Hönninger, Nicolas Dalloz, Anne Hildenbrand-Dhollande

Research Article Vol. 29, No. 5 / 1 March 2021 / Optics Express 6599
Optics EXPRESS

Diffraction limited 195-W continuous wave laser emission at 2.09 µm from a Tm^{3+}, Ho^{3+}-codoped single-oscillator monolithic fiber laser

ARNAUD MOTARD,[1,2,*] CHRISTOPHE LOUOT,[1] THIERRY ROBIN,[3] BENOIT CADIER,[3] INKA MANEK-HÖNNINGER,[2] NICOLAS DALLOZ,[1] AND ANNE HILDENBRAND-DHOLLANDE[1]

[1]*French-German research Institute of Saint-Louis, 68300 Saint-Louis, France*
[2]*Université Bordeaux, CNRS CEA, CELIA UMR5107, 33405 Talence, France*
[3]*Ixblue Photonics, 22300 Lannion, France*
[*]*arnaud.motard@isl.eu*

Abstract: We present a bi-directionally 793-nm diode-pumped Tm^{3+}, Ho^{3+}-codoped silica polarization maintaining double-clad all-fiber laser based on a single-oscillator architecture emitting 195 W at 2.09 µm in continuous wave mode of operation, with a beam quality near the diffraction limit ($M^2 = 1.08$). The power scaling of the laser is only pump-power-limited in the range of the total available pump power (540 W).

1. Introduction

The atmospheric transmission window around 2 µm is attracting much interest to fiber laser sources emitting at 2 µm for applications such as eye-safe surgery, material processing, or optical countermeasures [1–4]. The two most popular fiber laser architectures allowing power scalability at 2 µm are master oscillator power-amplifier (MOPA) fiber systems and single-oscillator fiber lasers. Monolithic fiber laser architectures delivering high powers around 2 µm have been largely demonstrated with MOPA systems [5–7]. Nevertheless, the high number of amplification stages needed to get a high average output power, and limitations due to MOPA laser physics (amplification stages isolation, ASE filtering, nonlinear effects) lead to relatively high complexity and volume for such laser sources [8]. Thanks to their high robustness, simpler structure and compactness, single-oscillator fiber lasers constitute one of the most promising architectures [9–11]. To date, 2 µm fiber lasers have been based predominantly on thulium-doped (Tm^{3+}) active media pumped at 793 nm, for efficient laser emission at 1.95µm wavelength [11–13]. Indeed, the energy transfer between the pumping at 793 nm and the 1.95 µm emission benefits a high efficiency via the $^3H_4$, $^3H_6 \rightarrow {}^3F_4$, $^3F_4$ cross-relaxation mechanism [14]. In 2016, Walbaum *et al*. demonstrated a monolithic single oscillator thulium-doped fiber laser delivering 567 W of output power at 1.97 µm with a slope efficiency of 49.4% with a M^2 factor of 2.7 [15]. To generate efficient radiations beyond 2 µm, a holmium-doped (Ho^{3+}) fiber can be pumped at 1.95 µm by a thulium-doped fiber laser. In 2013, Hemming *et al*. reported the highest output power from a holmium-doped fiber laser. A maximum output power of 407 W at 2.12 µm were obtained by using an array of six thulium-doped fiber pumping lasers operating at 1.95 µm [9]. In a way to reduce the laser system complexity while maintaining a good efficiency above 2 µm, a thulium-holmium-codoped fiber can be used as active medium in a laser source [16]. In 2020, Forster *et al*. demonstrated a thulium-holmium-codoped fiber laser source based on a free-space pumping scheme. A maximum output power of 181 W at 2.05 µm and a slope efficiency of 34.1% were achieved [17]. Nevertheless, free-space pumping systems suffer from difficult thermal management and optical alignments whereas a monolithic fiber laser, where all fiber-components

#416443 https://doi.org/10.1364/OE.416443
Journal © 2021 Received 2 Dec 2020; revised 5 Feb 2021; accepted 5 Feb 2021; published 17 Feb 2021

Optics EXPRESS

are fusion-spliced together, allows to have an alignment-free laser system offering a very stable and compact laser source.

In this paper, we present a monolithic single-oscillator laser source based on a Tm^{3+}, Ho^{3+}-codoped silica fiber emitting at 2.09 µm. This compact and all-fiber laser achieved a maximum output power of 195 W with a slope efficiency of 44.8% and an excellent beam quality near the diffraction limit ($M^2 < 1.1$).

2. Experimental setup

The experimental setup of the laser is shown in Fig. 1(a). The silica double-clad polarization maintaining (PM) fiber (iXblue Photonics) was 10 m long with a Tm^{3+}, Ho^{3+}-codoped core (diameter: 20 µm, numerical aperture NA = 0.11, Tm^{3+} ion concentration: 4 wt.%, Ho^{3+} ion concentration: 0.4 wt.%), surrounded by a Ge-doped pedestal, and a round-shaped cladding (diameter: 300 µm, numerical aperture: 0.46). The active fiber was symmetrically pumped by four high-power 793-nm fiber-coupled laser diodes, fusion-spliced to two 2 + 1×1 fiber pump combiners (FPCs) which directly inject the total pump power of 540 W into the active fiber. The high reflectivity (HR) mirror of the laser cavity was formed by a fiber Bragg grating (FBG) reflecting intracavity light at 2.09µm with a full-width-half-maximum (FWHM) bandwidth of 0.7 nm. The output coupler (OC) consisted of the FPC passive fiber cleaved at 0° (4-% Fresnel reflection). All the fibered components were fusion-spliced by a CO_2 splicer (LZM-100, Fujikura). The active fiber was coiled to a diameter of 17 cm and placed with the FBG into a thermal box where both were cooled by deionized water and kept at a constant temperature of 18 °C. A dichroic mirror was used at the output of the laser to filter the unabsorbed residual pump

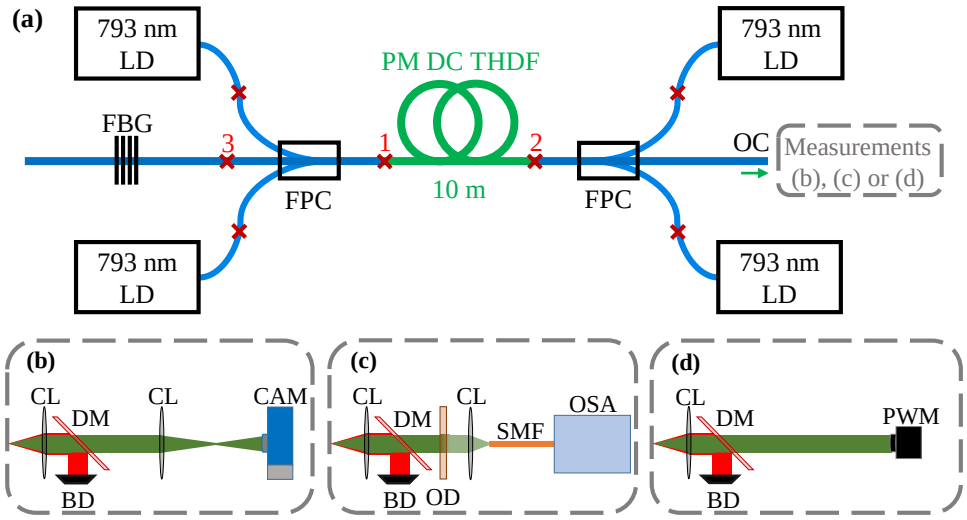

LEGEND

BD: Beam Dump, **CAM:** Camera Pyrocam III (*Spiricon, Ophir*), **CL:** Converging Lens, **DC:** Double Clad Fiber, **DM:** Dichroic Mirror, **FBG:** Fiber Bragg Grating, **FPC:** Fiber Pump Combiner, **LD:** Laser Diode, **OC:** Output Coupler, **OD:** Optical Density, **OSA:** Optical Spectrum Analyzer (*Yokogawa*), **PM:** Polarization Maintaining, **PWM:** Power Meter (*Nova, Ophir*), **SMF:** Single-Mode Fiber, **THDF:** Thulium-Holmium Co-doped Fiber.

Fig. 1. (a) Experimental setup for the monolithic single-oscillator fiber laser source. Passive and active fibers are represented in blue and green lines, respectively. Fiber fusion splices are represented by red crosses. Measurement setups for (b) spatial output profiles, (c) output spectrum, and (d) optical output power are depicted in the dashed-line boxes.

Optics EXPRESS

power and thus perform optical analyses on the 2.09 µm output signal. A complete analysis of the output signal, measuring the spatial profiles (Fig. 1(b)), the spectrum (Fig. 1(c)) and the optical power (Fig. 1(d)) was carried out.

3. Optimization of the laser intracavity splices

The intracavity splice quality does have a major impact on the laser performances (efficiency, beam quality, power handling, etc.). Therefore, all steps of the splicing process (stripping, cleaving and fusion-splicing) between fibers must be carefully optimized.

Firstly, we removed the coating fittingly in order to reduce the pump leakages at the interface between the coated and uncoated parts. Special attention has to be paid to properly remove all residuals of the coating, especially in order to avoid the formation of critical hot spots, which might cause the melting of the coating. Smaller hot spots can be supported at the power levels in our experiments. In a second step, the relative cleave angles have been maintained below 0.5° using a CT-106 Fujikura cleaver, in addition to a meticulous cleaning of both cleaved and stripped parts of the fiber tips. To quantify and measure the impact of the fusion parameters on the laser performances, investigations with an active splicing method have been carried out. This active splicing method consisted of visualizing in real time on the transmitted beam both the induced optical losses and beam profile degradations during the fusion-splicing process. The optimization of a splice was done by testing and adjusting different splicing parameters (fiber alignment method, arc duration, arc power, arc position, etc.) until we found the adapted parameters providing low optical losses and limiting beam profile degradations.

To optimize the active fiber splices 1 and 2 of the laser setup presented in Fig. 1, an external fiber laser source was developed (Fig. 2). This source was built with the same active fiber used in our setup (Fig. 1) pumped from one side by a single fiber-coupled laser diode at 793 nm. A single-clad passive fiber has been spliced to the active fiber in order to avoid multimode light propagation in the cladding and thus to keep only the light propagating in the fiber core. The amplified spontaneous emission (ASE) generated in the active fiber core of the external source was used as a reference beam for all the analyses. As this single-clad passive fiber has exactly the same core/cladding properties of the double-clad passive fiber used in the FPC (only the coating differs), this fiber can be used to optimize the splicing parameters between the active fiber and the DC passive fiber in approach to the splices at the FPCs as shown in Fig. 1. As the development of a dedicated splicing program can be fiber consuming, splicing tests were realized between fiber samples for both the active and the passive fibers. Once the optimized splicing program was developed, the fiber samples were replaced by the active fiber and the FPCs as depicted in Fig. 1.

Three analyses were performed simultaneously: (i) the pump leakage at the splice interface was visualized thanks to the LZM-100 splicer's internal cameras; (ii) the power losses generated by the splice process were estimated by measuring the power at the output of the passive fiber; (iii) the beam profile was observed in order to detect any degradation during splicing.

With this active splicing analysis, we highlighted that the pump losses at the splice interface can be greatly reduced by heating again the splice during a few seconds with a CO_2 laser power approximately 2 times lower than the power used for splicing. Figure 3 shows photographs of the longitudinal view in x and y direction of a splice before (Fig. 3(a)) and after (Fig. 3(b)) second heating. As represented on Fig. 3(a), the splicer's cameras were saturated after the splice by the leaking pump power, whereas the new heating made the leakage almost disappear (Fig. 3(b)).

The active splicing process is also used to qualitatively assess the degradation on the transmitted beam at a wavelength of 2.09 µm and to measure the power losses caused by the fusion-splice between the two fibers. The LZM-100 splicer starts the splicing procedure by automatically aligning the two fibers together. This aligned-fiber configuration is used as a reference both for the transmitted beam profile and the output power at a wavelength of 2.09 µm. The two fibers are then aligned, in face-to-face, as shown in the longitudinal view in x and y direction in Fig. 4.

Optics EXPRESS

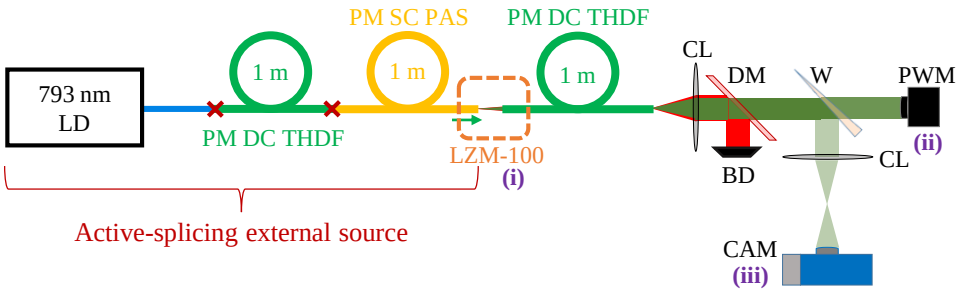

LEGEND

BD: Beam Dump, **CAM:** Camera Pyrocam III (*Spiricon*, *Ophir*), **CL:** Converging Lens, **DC:** Double Clad Fiber, **DM:** Dichroic Mirror, **LD:** Laser Diode, **LZM-100:** Fusion-splicing system (*Fujikura*), **PAS:** Passive fiber, **PM:** Polarization Maintaining, **PWM:** Power Meter (*Nova*, *Ophir*), **SC:** Single Clad Fiber, **THDF:** Thulium-Holmium Doped Fiber, **W:** Wedge.
(i) pump leakage visualization, **(ii)** optical output power measurement, **(iii)** output spatial profiles measurement.

Fig. 2. Experimental setup for active splicing. Active, single-clad passive fibers are represented in green and yellow lines, respectively. Fiber fusion-splices are represented by red crosses.

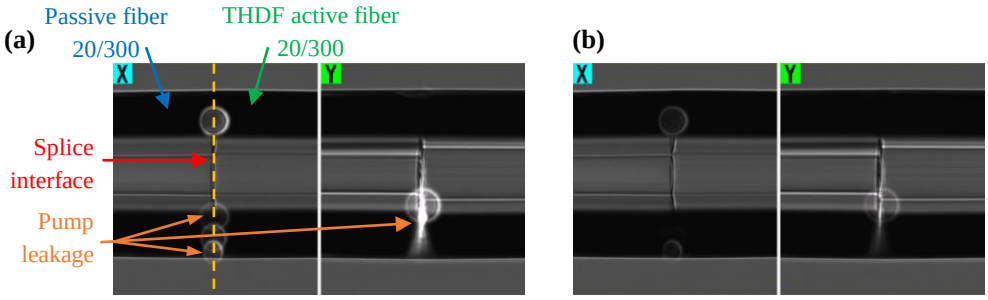

Fig. 3. Longitudinal views in x and y direction of the splice between the passive fiber and the active fiber: (a) before a second heating; (b) after a second heating.

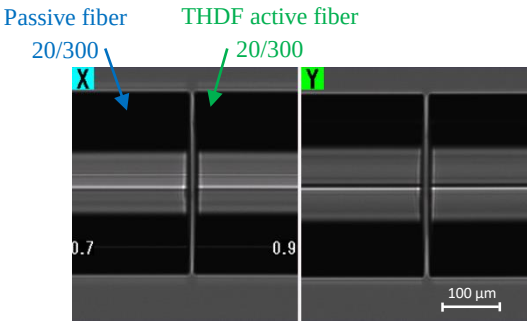

Fig. 4. Longitudinal view in x and y direction of the fibers in a face-to-face configuration after alignment and before splicing.

Optics EXPRESS

Figure 5 presents the transversal beam profile obtained during two active splicing processes using an inadequate (Fig. 5(a)) and an adapted (Fig. 5(b)) splicing set of parameters. In each case, the beam profile after splicing is compared to the reference beam (i.e. the beam emitted by the external source), both by qualitative analysis of visual degradation of the profile and by splice loss measurements. In the case of inadequate parameters, we can clearly observe an important distortion on the beam profile associated with high-power losses (47%). The improvement of the splice by choosing adapted parameters gives a better light transmission through the splice with only 1.5% of power losses and no more profile degradation.

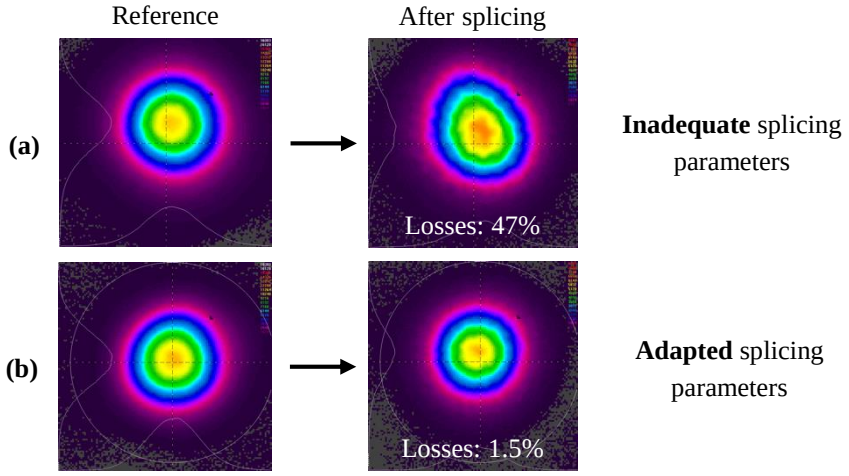

Fig. 5. Examples of two active splicing processes using an inadequate (a) and an adapted (b) splicing set of parameters. The reference beams (on the left) and the transmitted beams after-splicing (on the right) are shown for each splice with the power losses measured at a wavelength of 2 µm.

Once the active fiber splices have been performed, an active splicing method has also been applied for the splice between the FBG and the FPC (splice 3 in Fig. 1). In that case, the ASE beam emitted in both directions by the active fiber core (when pumped by the 793-nm fiber-coupled diodes) has been used as a reference to fusion-splice the FBG on the FPC. The optimization procedure was the same as the one described here above.

4. Results and discussion

The output power of the fiber laser as a function of the total injected pump power is shown in Fig. 6. A maximum continuous wave (CW) output power of 195 W has been achieved at 2.09µm, with 44.8% slope efficiency and 39 W power threshold for 472 W of maximum injected pump power (12% pump insertion losses in combiners). To the best of our knowledge, this is the highest output power demonstrated from a monolithic single-oscillator fiber laser source based on a Tm^{3+}, Ho^{3+}-codoped silica fiber. The power increase was only limited by the available pump power.

One can notice that the demonstrated 45% slope efficiency is above the Stokes efficiency limit of ~38% imposed by the quantum defect of this fiber laser [13]. This result indicates that the thulium ion concentration of 4 wt.% of the fiber core is high enough to generate a two-for-one cross relaxation process with the 793-nm pumping, and that maintaining a Tm/Ho concentration ratio of 10 leads to a good energy transfer from Tm^{3+} to Ho^{3+} ions [18]. Ramírez-Martínez *et al.* have demonstrated in [18] a slope efficiency of 56% for a Tm^{3+}, Ho^{3+}-codoped single-oscillator fiber laser. This record efficiency was obtained for a fiber laser architecture based on a free-running

Optics EXPRESS

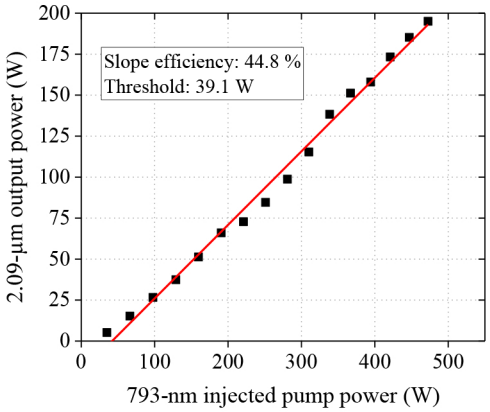

Fig. 6. 2.09-µm continuous wave output power versus 793-nm incident pump power.

cavity, with 4-% Fresnel reflections on both 0°-cleaved-angle active fiber tips (no spectral filtering component in the cavity), and a 793-nm free-space symmetrical pumping scheme.

Figure 7 depicts two typical beam quality factor measurements, one at low output power of 15 W (Fig. 7(a)) and the other at the maximum output power of 195 W (Fig. 7(b)). The beam radius was measured with a Pyrocam III HR camera (Spiricon, Ophir) according to the D4σ formalism. A fitting of the beam propagation equations allows us to determine the beam quality factors. At 15 W of output power, the M^2 factors were estimated to be 1.06 and 1.07 in the x and y directions, respectively. At the maximum output power, the M^2 is 1.07 in x direction and 1.09 in y direction. Note that due to our setup, we could not measure enough points outside the Rayleigh range conforming to the ISO 11146-1 which limits the accuracy of the result. These results indicate that the fiber laser operates near the diffraction limit over the entire power scaling. The insets in Fig. 7 show the transverse beam profiles for two relative propagation distances. The signal light was not stripped from the cladding since it seems to us to be very low compared to the power of the fundamental mode according to the beam profile measurements.

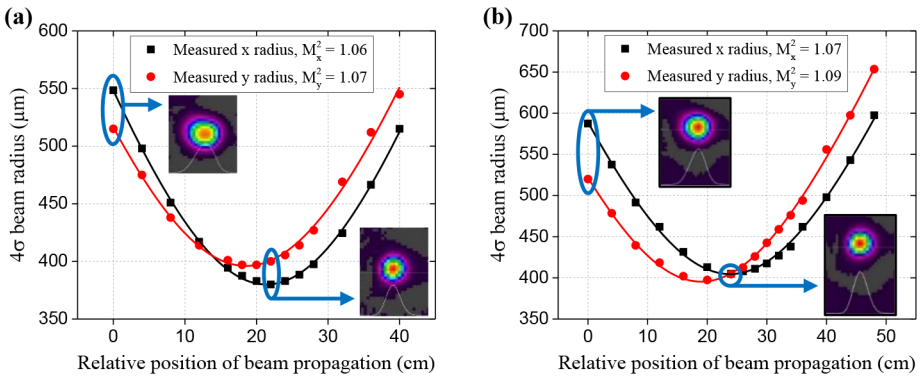

Fig. 7. Measured caustic of the focused laser output beam and derived M^2 beam quality factors at 15 W of output power (a) and at the maximum output power (195 W) (b). The insets show the transverse beam profiles measured with a Pyrocam III HR camera for two relative propagation distances.

Optics EXPRESS

Figure 8(a) shows the main laser peak spectrum of the output beam measured by an Optical Spectrum Analyzer (OSA, Yokogawa) with a wavelength resolution of 0.01 nm at two different output power levels, one at 15 W (black curve) and the other at 195 W (red curve). At 15 W, the spectral full width at half maximum (FWHM) was 0.6 nm at a central wavelength of 2090.0 nm, whereas at the maximum output power, the spectral bandwidth was 1.2 nm and centered at 2092.4 nm. One can thus notice a spectral shift of 2.4 nm and a spectral broadening of 0.6 nm when increasing the power. The spectral shift is due to the FBG heating, despite its position in a thermal box cooled at 18 °C [19]. The spectral broadening arises from nonlinear effects occurring with high light intensity [20]. Even if the spectral linewidth doubles when rising the power it remains a relatively narrow spectrum (~1 nm) which should not be a problem for the applications mentioned in the introduction. The spectral shift of 2.4 nm at maximum output power to the higher wavelengths would also not be an issue for most of the targeted applications. Moreover, the shift could be taken into account by using a fiber Bragg grating with a lower reflectivity wavelength in order to emit at the desired central wavelength for a specific power. Additionally, it would be possible to limit these effects of spectral shifting and broadening by using an active cooling system only dedicated to the FBG thermalization. Figure 8(b) shows that the output power spectrum measured at maximum power (red line) is presenting several peaks: one main lasing peak of $\delta\lambda_1 = 0.5$ nm linewidth, and several side peaks periodically separated by $\delta\lambda_2 = 0.3$ nm. We assume that this specific shape of the output power spectrum could be the result of spectral filtering mechanisms arising from the FBG. Indeed, the high power broadband intracavity power spectrum, measured to be 1.2 nm large at the output of the fiber laser, is spectrally overlapping the 0.7 nm reflection bandwidth when propagating back to the FBG. Consequently, since the reflectivity spectrum of a FBG presents periodically-separated side lobes [21], the intracavity power spectrum reflected by the FBG should present side peaks which are power-amplified when propagating again through the active fiber of this laser source.

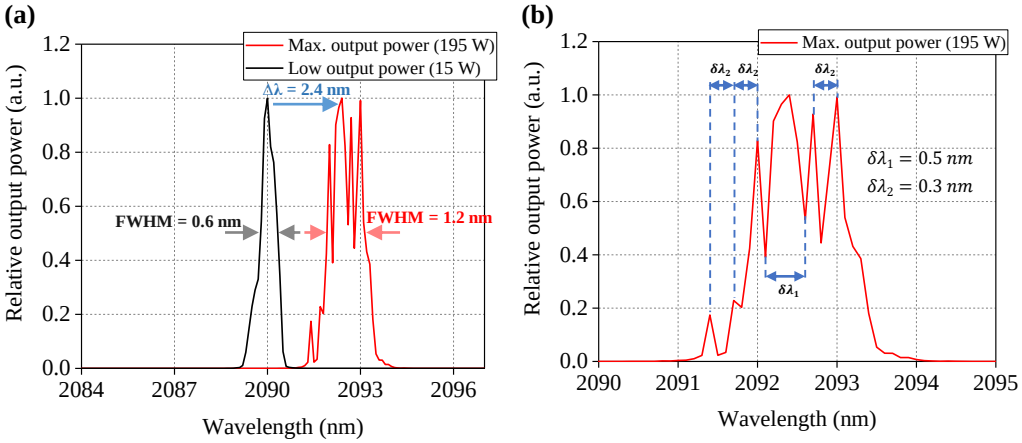

Fig. 8. (a) Laser emission spectra measured at 15 W (black curve) and 195 W (red curve) output power. (b) Zoom in the laser emission spectrum measured at 195 W output power.

Figure 9(a) shows the whole signal spectrum of the output beam measured by the OSA at an output power of 195 W. A large wavelength range is now used in order to observe the multitude of secondary peaks located around 2115 nm, which had a relative maximum power level of −15 dB with respect to the main peak. To understand the physical origin of these secondary peaks, Fig. 9(b) shows the signal spectrum of the output beam for different 793-nm pump power after removing the FBG from the laser. In this configuration, the laser architecture was based on a free-running cavity (4-% Fresnel reflections on both sides). Below a threshold comprised

Optics EXPRESS

between 30 W and 33 W of pump power, we can see the broadband ASE spectrum emitted by the fiber laser. However, above this power threshold, we can clearly observe a laser emission peak at 2115 nm, i.e. at the same wavelength range of the secondary peaks observed in Fig. 9(a). Thus, when the emission wavelength is not imposed by a FBG, the natural emission of our fiber laser, corresponding to the maximum absorption gain, is around 2115 nm when using a 10-m piece of Tm^{3+}, Ho^{3+}-codoped fiber. Therefore, the secondary peaks observed around 2115 nm at the output of the fiber laser in the configuration depicted in Fig. 1 are due to the presence of a maximum gain at this wavelength. This conclusion suggests that the amplifier efficiency may be improved by using a FBG at 2115 nm instead of 2090 nm, or by using a more adapted fiber length in order to have the maximum absorption gain at the same wavelength as the reflectivity of the FBG. This would also allow for further pump power increase without limitation caused by the secondary peaks of emission.

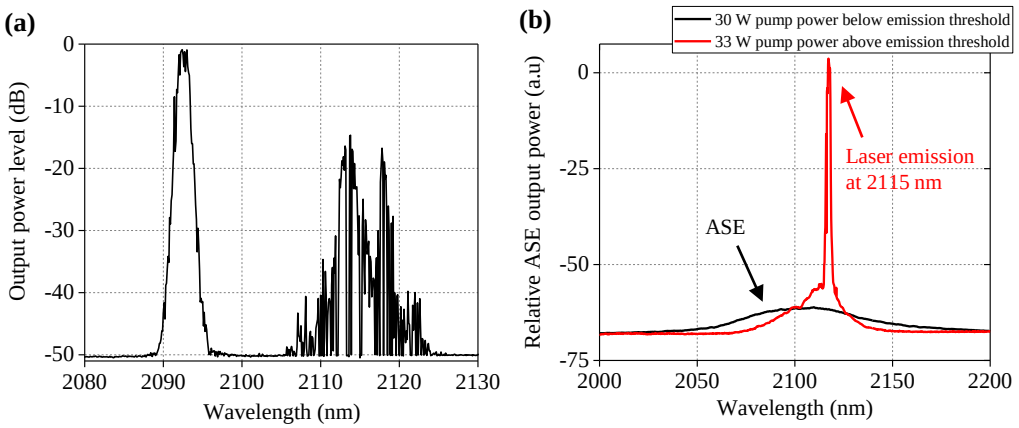

Fig. 9. (a) Large span laser emission spectrum measured at 195-W output power to see the secondary peaks. (b) Output spectrum of the free-running-cavity fiber laser (without FBG) around its laser emission power threshold.

5. Conclusions

In conclusion, we demonstrated a single-oscillator Tm^{3+}, Ho^{3+}-codoped silica PM double-clad all-fiber laser. With this fiber laser, 195 W of output power at 2.09 µm wavelength in CW mode of operation with a spectral linewidth of 1.2 nm and a beam quality factor of 1.08 was obtained. The slope efficiency was 44.8% for a power threshold of 39 W. The maximum output power was currently limited in the range of the total available pump power. To the best of our knowledge, this is the most powerful monolithic single-oscillator laser source based on a Tm^{3+}, Ho^{3+}-codoped silica fiber demonstrated in the literature.

Disclosures. The authors declare no conflicts of interest.

References

1. L. Wang, Z. Wang, B. Yang, Q. Yang, and Y. Sun, "Thulium laser urethrotomy for urethral stricture: A preliminary report," Lasers Surg. Med. **42**(7), 620–623 (2010).
2. I. Mingareev, F. Weirauch, A. Olowinsky, L. Shah, P. Kadwani, and M. Richardson, "Welding of polymers using a 2µm thulium fiber laser," Opt. Laser Technol. **44**(7), 2095–2099 (2012).
3. D. H. Titterton, "Military Laser Technology and Systems," (Artech House, 2015).
4. N. Dalloz, T. Robin, B. Cadier, C. Kieleck, M. Eichhorn, and A. Hildenbrand-Dhollande, "55 W actively Q-switched single oscillator Tm^{3+}, Ho^{3+}-codoped silica polarization maintaining 2.09 µm fiber laser," Opt. Express **27**(6), 8387–8394 (2019).
5. T. Ehrenreich, R. Leveille, I. Majid, K. Tankala, G. Rines, and P. Moulton, "*1-kW, all-glass Tm:fiber laser*," presented at SPIE Photonics West: LASE, San Francisco, USA (2010).

Optics EXPRESS

6. J. Liu, H. Shi, K. Liu, Y. Hou, and P. Wang, "210 W single-frequency, single-polarization, thulium-doped all-fiber MOPA," Opt. Express **22**(11), 13572–13578 (2014).
7. R. E. Tench, C. Romano, and J.-M. Delavaux, "A 25 W 2 µm broadband polarization-maintaining hybrid Ho- and Tm-doped fiber amplifier," Appl. Opt. **58**(15), 4170–4175 (2019).
8. W. Yao, C. Shen, Z. Shao, J. Wang, F. Wang, Y. Zhao, and D. Shen, "790 W incoherent beam combination of a Tm-doped fiber laser at 1941nm using a 3×1 signal combiner," Appl. Opt. **57**(20), 5574–5577 (2018).
9. A. Hemming, N. Simakov, A. Davidson, S. Bennetts, M. Hughes, N. Carmody, P. Davies, L. Corena, D. Stepanov, J. Haub, R. Swain, and A. Carter, "A monolithic cladding pumped holmium-doped fiber laser," *Conference on Lasers and Electro-Optics, OSA Technical Digest* (Optical Society of America, 2013), paper CW1M.1.
10. A. Hemming, N. Simakov, M. Oermann, A. Carter, and J. Haub, "Record efficiency of a holmium-doped silica fibre laser," *Conference on Lasers and Electro-Optics, OSA Technical Digest* (Optical Society of America, 2016), paper SM3Q.5.
11. D. Pal, A. Ghosh, R. Sen, and A. Pal, "Continuous-wave and quasi continuous-wave thulium-doped all fiber laser: implementation on kidney stone fragmentations," Appl. Opt. **55**(23), 6151–6155 (2016).
12. L. Shah, R. A. Sims, P. Kadwani, C. C. Willis, J. B. Bradford, A. Sincore, and M. Richardson, "High-power spectral beam combining of linearly polarized Tm:fiber lasers," Appl. Opt. **54**(4), 757–762 (2015).
13. Q. Tan, T. Ge, X. Zhang, and Z. Wang, "Cascaded combiners for a high power CW fiber laser," Laser Phys. **26**(2), 025102 (2016).
14. S. D. Jackson, "Cross relaxation and energy transfer upconversion processes relevant to the functioning of 2 µm Tm^{3+} -doped silica fiber lasers," Opt. Commun. **230**(1-3), 197–203 (2004).
15. T. Walbaum, M. Heinzig, T. Schreiber, R. Eberhardt, and A. Tünnermann, "Monolithic thulium fiber laser with 567 W output power at 1970nm," Opt. Lett. **41**(11), 2632 (2016).
16. S. D. Jackson, A. Sabella, A. Hemming, S. Bennetts, and D. G. Lancaster, "High-power 83 W holmium-doped silica fiber laser operating with high beam quality," Opt. Lett. **32**(3), 241 (2007).
17. P. Forster, C. Romano, C. Kieleck, and M. Eichhorn, "Advances in two-micron lasers for nonlinear conversion into the mid-IR," Proc. SPIE **11355**, 10 (2020).
18. N. J. Ramírez-Martínez, M. Núñez-Velázquez, and J. K. Sahu, "Study on the dopant concentration ratio in thulium-holmium doped silica fibers for lasing at 2.1µm," Opt. Express **28**(17), 24961–24967 (2020).
19. G. Meltz and W. W. Morey, "Bragg grating formation and germanosilicate fiber photosensitivity," *Proc. SPIE* 1516, (1991).
20. G. P. Agrawal, "*Nonlinear Fiber Optics*," (Academic Press, 1995).
21. T. Erdogan, "Fiber Grating Spectra," J. Lightwave Technol. **15**(8), 1277–1294 (1997).